Journal of Photochemistry & Photobiology, B: Biology 162 (2016) 34–44

Contents lists available at ScienceDirect

Journal of Photochemistry & Photobiology, B: Biology

journal homepage: www.elsevier.com/locate/jphotobiol

A novel Schiff base derived from the gabapentin drug and copper (II) complex: Synthesis, characterization, interaction with DNA/protein and cytotoxic activity

Zahra Shokohi-pour [a], Hossein Chiniforoshan [a,*], Amir Abbas Momtazi-borojeni [b], Behrouz Notash [c]

[a] Department of Chemistry, Isfahan University of Technology, Isfahan, Iran, 84156-83111
[b] Student Research Committee, Nanotechnology Research Center, Department of Medical Biotechnology, School of Medicine, Mashhad University of Medical Sciences, Mashhad, Iran
[c] Department of Chemistry, Shahid Beheshti University, G. C., Evin, Tehran 1983963113, Iran

ARTICLE INFO

Article history:
Received 6 January 2016
Received in revised form 12 June 2016
Accepted 13 June 2016
Available online 15 June 2016

Keywords:
Schiff base
Copper (II) complex
Gabapentin
Interaction with DNA and BSA
Cytotoxic activity

ABSTRACT

A novel Schiff base [$C_{20}H_{23}NO_3$], has been prepared and characterized using FT-IR, UV–vis, ^{1}H NMR spectroscopy, elemental analysis and X-ray crystallography. A copper (II) complex [$Cu(C_{20}H_{22}NO_3)_2]\cdot H_2O$ has also been synthesized and characterized. The new ligand and complex thus obtained were investigated by their interaction with calf thymus DNA and BSA using electronic absorption spectroscopy, fluorescence spectroscopy, and thermal denaturation. The intrinsic binding constants K_b of the ligand and Cu (II) complex, with CT-DNA obtained from UV–vis absorption studies were 1.53×10^4 M^{-1} and 3.71×10^5 M^{-1}, respectively. Moreover the addition of the two compounds to CT-DNA (1:2) led to an increase of the melting temperature of DNA up to around 2.61 °C for the ligand and 3.99 °C for the Cu (II) complex. The ligand and Cu (II) complex bind to CT-DNA via a partial intercalative, as shown by the experimental data. In addition, the albumin interactions of the two compounds were studied by fluorescence quenching spectra, the results indicating that the binding mechanism is a static quenching process. The in vitro cytotoxicity of the two compounds on three different cancer cell lines was evaluated by MTT assay. The results showed that the copper complex exerted enhanced cytotoxicity compared with the Schiff base ligand; thereby, this complex clearly implies a positive synergistic effect. Furthermore, the copper complex showed a high, selective, and dose-dependent cytotoxicity against cancer cell lines.

1. Introduction

Gabapentin, 1-(aminomethyl) cyclohexaneacetic acid, Neuronti (Gpn) structurally belongs to the neurotransmitter gamma-aminobutyric acid (GABA), widely studied for its significant inhibitory action in the central nervous system [1]. Gpn has been applied in the treatment of neuropathic pain. It is a new generation antiepileptic used as add-on therapy and monotherapy in patients with partial seizures [2]. A safe and effective seizure is a concern for an increasing number of adults suffering from epilepsy. Epilepsy also imposes a remarkable economic load on society [3]. The selection of an antiepileptic drug depends on how it functions with regard to the specific seizure type, tolerability, and safety. Furthermore, gabapentin can be considered as an emergent solution for the "pain riddle". Starting from this point, more randomized, double blind studies, which compare analgesic drugs with gabapentin, may be relevant to identifying the first choice therapy for acute and chronic pain relief [4]. Thus, the search for novel chemical entities for the cure of epilepsy is essential [5,6]. Usually formed by condensation of a primary amine with an active carbonyl compound, Schiff bases are compounds containing the azomethine group (R—C═N). The biological activities and decreased cytotoxicity of both metal ion and Schiff base ligand are due to the attachment of transition metals in to these compounds [7–9]. Considering their great flexibility and various structural aspects, a wide range of transition metal complexes of Schiff base ligands have been synthesized and the structure function relationships of the resulting complexes have been extensively focused on in recent years [10–14]. Piotr et al. have synthesized various compounds such as amino thiazoles, 2-hydroxy-1-napthalaniline, amino sugars, aromatic aldehydes, ketones, thiosemicarbazides, amino acids, pyrazolone, etc. [15]. Recently, some novel coordination compounds based on Schiff base ligands were found useful as potential pro drugs. Consequently, transition metal complexes of Schiff bases have been extensively studied as promising alternatives to traditional cisplatin for anticancer drugs. In addition, Schiff base complexes have attracted much attention given their important role in the improvement of novel therapeutic agents and novel nucleic acid structural probes [16]. DNA is an essential cellular receptor and is the primary target molecule for most anticancer and antiviral therapies. Many compounds apply their anticancer effects via binding

* Corresponding author.
E-mail address: chinif@cc.iut.ac.ir (H. Chiniforoshan).

http://dx.doi.org/10.1016/j.jphotobiol.2016.06.022

to DNA, thereby changing DNA replication and inhibiting the growth of the tumor cells, which is the basis for designing new, more effective anticancer drugs, the efficacy of which depends on the mode and tendency of the binding [17]. Revealing the features leading to increased DNA binding capability by small ligands or metal complexes is important for designing efficient chemotherapeutic agents and better DNA targeted anticancer drugs [18]. Therefore, the DNA-binding studies of small metal complexes are very significant in the improvement of new anticancer drugs [19,20]. Moreover, naphthaldehyde Schiff base ligand, an aromatic planar ligand with carbonyl O and N donor atoms, can coordinate to metal ions to form metal intercalators, which show strong intercalation with DNA. The selection of a metal ion is the most significant factor in the design of a metal based chemotherapeutic agent [21]. Copper is a crucial cofactor in tumor angiogenesis processes and is a bioessential and bio-relevant element, which is an inseparable component of many enzymes, including superoxide dismutase, tyrosinase, ceruloplasmin, etc. [22,23]. Many copper (II) complexes with biological activities such as antibacterial, anti-cancer and cancer inhibiting properties have already been dealt with in the literature [24,25]. Palaniandavar and co-workers have reported that copper (II) complexes are the best alternatives to cisplatin because copper plays many significant parts in biological systems and is a biocompatible metal [26], considering the strong interactions of copper complexes with DNA through surface associations or intercalation [27]. Moreover, the investigation of the interactions of novel copper (II) Schiff base complexes with DNA is greatly important for disease defense, new medicine design and clinical application of drugs [28]. A copper complex has been synthesized from gabapentin drug Schiff base and the corresponding biological properties such as DNA binding, protein binding, and in vitro cytotoxicity have been studied. One of the important properties of a drug is its protein binding degree, affecting its effective solubility, biodistribution, and half life in the body [29]. Biomolecule proteins play an important role in transportation and deposition of endogenous and exogenous substances including fatty acids, hormones, and drugs. They also have many physiological functions. BSA, bovine serum albumin, is often selected as a target protein to study interactions with small molecules due to its low cost, ready accessibility and similarity to human serum albumin [30]. A stable protein drug complex with a dominant role in storage and drug disposition may be formed by a significant interaction of any drug with a protein. Therefore, understanding the mechanism of interaction of a bioactive compound with BSA, a well studied protein, is important [31]. A new Schiff base derived from the gabapentin drug and copper complex has been studied in this work from four aspects; (i) synthesis and characterization of the ligand and complex using spectroscopy and X-ray diffraction, (ii) study of the ability of the two compounds to interact with DNA and the interaction mechanism using UV–vis, fluorescence spectroscopy, and thermal denaturation, (iii) monitoring of the protein binding ability by UV absorption and tryptophan fluorescence quenching experiment in the presence of the two compounds using BSA as a model protein, and (iv) a comparative study of the in vitro cytotoxicity of the three compounds on three human carcinomas (JURKAT, SKOV3, and U87) and peripheral blood mononuclear cell (PBMC) by MTT assay.

2. Experimental

2.1. Materials

All chemicals and solvents used for synthesis were commercially available, reagent grade and were used without further purification. Solvents and starting materials were supplied by Sigma Aldrich or Alfa Aesar Chemical Companies and used without further purification. BSA and Calf thymus DNA (CT-DNA) were purchased from Sigma Aldrich Chemical Company and were used as supplied. The DNA concentration per nucleotide was determined by absorption spectroscopy using the molar absorption coefficient ($\varepsilon = 6600\ M^{-1}\ cm^{-1}$ at 260 nm) [32]. The stock solutions were stored at 5 °C and used over a period of 4 days. All the experiments involving interactions of the compounds with DNA were performed using doubly distilled water buffer containing 5 Mm Tris–HCl [tris (hydroxymethyl)-aminomethane] and 50 mM NaCl, adjusted to pH 7.4 using hydrochloric acid. Ligand and Cu complex stock solutions were prepared by dissolving the two compounds in water and DMSO as the co-solvent, and then diluted with the corresponding buffer to the necessary concentrations for all the experiments. The final DMSO concentration did not exceed 0.5% v/v. JURKAT (human leukemic T cell line), SKOV3 (human ovarian cancer cell line), U87 (human glioblastoma cell line), and PBMC (peripheral blood mononuclear cell) were supplied by the National Cell Bank of Pasteur Institute, Tehran, Iran. Cells were cultured in Dulbecco's Modified Eagle Medium (DMEM) supplemented with 10% heat inactivated fetal bovine serum (FBS), 100 U ml^{-1} penicillin, 100 μg ml^{-1} streptomycin and 5 mM L-glutamine. The cell lines were subsequently grown at 37 °C in a humidified atmosphere containing 5% CO_2. All reagents and cell culture media were purchased from Gibco Company (Germany).

2.2. Physical Measurements

Fourier transform infrared (FT-IR) spectra were recorded as KBr disks on an FT-IR JASCO-680 spectrophotometer in the 4000–400 cm^{-1} ranges using the KBr pellets technique. The elemental analyses were performed on a Leco, CHNS-932 apparatus. UV–vis spectra were recorded on a JASCO V-570 spectrophotometer in the 190–900 nm range. NMR spectra were measured on a Bruker spectrometer at 400.13 MHz. The T_m spectra were recorded on a Varian BioCary-100 UV–vis spectrophotometer using a 1 cm path length cell. Solutions were prepared by dissolving the complex in water buffer containing 5 mM Tris–HCl (pH 7.4) and 50 mM NaCl. Electrospray mass spectra were obtained using a Shimadzu LCMS-2010 EV liquid chromatography mass spectrometer.

2.3. Synthesis of the Schiff Base Ligand

The Schiff base ligand, was prepared by equimolar (1:1 mol ratio) condensation between gabapentin (0.160 g, 1 mmol) and 2-hydroxy1-naphthaldehyde (0.172 g, 1 mmol) by stirring for 3 h at room temperature in absolute ethanol and recrystallization using absolute methanol by slow evaporation. Ligand yield (86%) (0.75 mg); color: yellow; MP: 215 °C; anal., calc. for, [$C_{20}H_{23}NO_3$]; C, 73.82; H, 7.12; N, 4.30; O, 14.75%. Found; C, 73.50; H, 7.24; N, 4.35; O, 14.90%. FT-IR (KBr, cm^{-1}): 3436 ν (O—H), 2929 and 2855 ν (C—H), 1690 ν_{as} (COO^-), 1638 ν (C═N), 1545 ν (C═C), 1359 ν_s (COO^-) 0.1030 ν (C—O), 964 ν (C—N)·^{1}H NMR ($CDCl_3$, δ, ppm): 8.43 (s, 1H, HC═N), 7.65–7.67 (d, 1H^a, Ar—H, $^3J = 8.3$), 7.53–7.55 (d, 1H^b, Ar—H, $^3J = 7.1$), 7.47–7.49 (d, 1H^c, Ar—H, $^3J = 9.2$), 7.29–7.32 (t, 1H^d, Ar—H $^3J = 7.5$), 7.10–7.14 (t, 1H^e, Ar—H $^3J = 7.4$) 6.76–6.79 (d, 1H^f, Ar—H, $^3J = 9.2$) 3.50 (s, 2H, CH_2), 2.30 (s, 2H CH_2), 1.39–1.78 (m, 10H, cyclohexyl methylenes group). UV–vis (solvent methanol λ_{max}, nm (ε, $M^{-1}\ cm^{-1}$)): 232 (1.82×10^4), 310 (4.50×10^3), 394 (5.68×10^3).

2.4. Synthesis of $[Cu(C_{20}H_{22}NO_3)_2]\cdot H_2O$

The synthesis of copper complex is as follows: copper (II) acetate tetrahydrate (0.249 g, 1.0 mmol) and ligand (0.620 g, 2.0 mmol) were added to a 40 mL methanolic solution and stirred for 5 h. The formed Cu (II) complex was filtered and washed with diethyl ether.

Copper (II) complex $[Cu(C_{20}H_{22}NO_3)_2]\cdot H_2O$, yield (90%), color: light green; MP: 365 °C; anal., calc. for $C_{40}H_{46}CuN_2O_7$: C, 65.78; H, 6.35; N, 3.84; O, 13.48%. Found; C, 65.22; H, 6.53; N, 3.77%; O, 13.36%. FT-IR (KBr, cm^{-1}) 3382 ν (O—H), 2924 and 2856 ν (C—H), 1600 ν (C═N), 1549 ν_{as} (COO), 1509 ν (C═C), 1310 ν_s (COO), 1048 ν (C—OH), 961 ν (C—N),458 ν (Cu—N) and 541 ν (Cu—O). UV–vis (solvent methanol

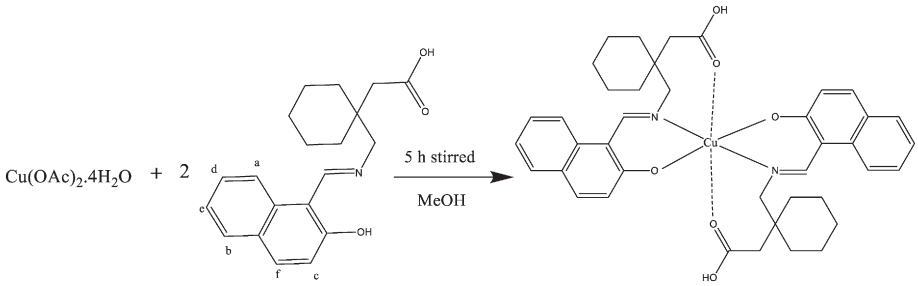

Scheme 1. Synthesis of the copper (II) complex.

λ_{max}, nm (ε, M^{-1} cm^{-1}): 240 (2.81×10^4), 310 (1.09×10^3), 376 (8.40×10^3), 678 (1.60×10^2). ESI-MASS: 713.45.

3. Results and Discussion

3.1. Synthesis and Spectroscopic Characterization

In this study, 2-hydroxy-1-naphtaldehyde was used to react with gabapentin and a novel Schiff base was synthesized from the gabapentin drug. In addition, copper (II) complex is obtained in one step by the reaction of [Cu $(OAc)_2]\cdot 4H_2O$ with ligand in MeOH under stirring for 5 h (Scheme 1). The compound was characterized by FT-IR spectroscopy, elemental analysis (C, H, N), and UV–vis spectral studies. The ESI–MS studies confirmed the formula proposed for the copper complex.

3.1.1. Infrared Spectra

The FT-IR spectra of the Schiff base ligand and copper (II) complex exhibit several bands in the 400–4000 cm^{-1} region (Sections 2.3–2.4). The azomethine vibration of the Schiff base ligand appeared at 1639 cm^{-1}. Because of bond formation between the metal and the imine nitrogen, the C═N bond stretching was shifted to lower frequencies relative to the free Schiff base and appeared at 1600 cm^{-1} for the copper complex [33]. The $\Delta\nu = [\nu_{as}(CO_2) - \nu_s(CO_2)]$ value was used to determine the nature of binding of carboxylate to a transition metal ion. In general, the difference in $\Delta\nu$ between asymmetric and symmetric $\nu_s(CO_2)$ absorption frequencies below 200 cm^{-1} suggests the bidentate carboxylate moiety while absorption frequencies >200 cm^{-1} implicate unidentate carboxylation. In the copper complex, the $\Delta\nu$ values were above 239 cm^{-1} suggestive of coordination of the carboxylate group in a monodendate fashion [34]. In the Cu (II) complex, these can be assigned to the ligand coordinated to the metal ion via imine nitrogen, phenolic oxygen and oxygen carboxylic acid atoms. Moreover, the formation of a copper complex was also revealed by the presence of medium intensity ν (M–N) and ν (M–O) bands at about 458 and 541 cm^{-1}, respectively, in the far IR region [35].

3.1.2. Electronic Absorption Spectra

The UV–vis spectral data (300–800 nm) of the ligand and synthesized complex are shown in Sections 2.3–2.4. The Schiff base ligand exhibits electronic transitions with a strong band at 232 nm, assigned to π–π* transitions [36]. The transition at 310 nm is assigned to the π–π* type and the band at 394 nm involves π–π* transition related to the azomethine group. The band at 394 nm was shifted to lower wavelengths and appeared at about 376 nm mixed with charge transfer transition. In addition, the bands around 376 nm are assigned to metal-to-ligand charge transfer (MLCT) transitions [37]. The spectral similarity suggests that all the complexes present the same chromophore in solution. The complex revealed d–d transitions in the lower frequency region centered at 678 nm and a band in UV region at 240 nm consistent with their octahedral geometry, respectively. Moreover, the distorted octahedral Cu (II) complex displays one band at 678 nm, corresponding to $^2E_g \rightarrow {}^2T_{2g}$ ($^2B_{1g} \rightarrow {}^2E_g$)) transition [38].

3.1.3. Mass Spectroscopy

The formation of copper complex and the speciation of various ionic forms in DMSO/MeOH solution were studied with ESI–MS. The spectra of the complex displayed prominent peaks corresponding to the

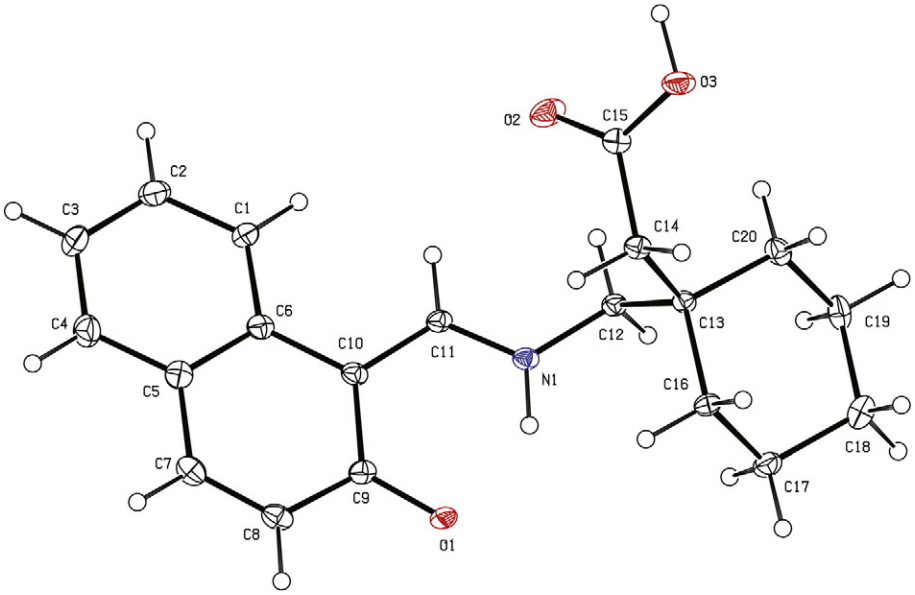

Fig 1. The labeled ORTEP diagram of Schiff base ligand. Thermal ellipsoids are at 30% probability level.

molecular ion fragment (Supplementary material Fig. S1a, S1b). The complex showed a peak at m/z^+ 713.45 corresponding to the $[C_{40}H_{44}CuN_2O_6 + 2H]$ fragment. The molecular formulae assigned to these complexes are further supported by ESI-mass studies.

3.1.4. Crystal Structure of the Ligand

3.1.4.1. Crystal Structure Determination and Refinement. Crystals of a Schiff base ligand suitable for X-ray crystallography were obtained from methanol solution at room temperature. The X-ray diffraction measurements were made on a STOE IPDS-2 T diffract meter with graphite monochromated Mo-Kα radiation. For the Schiff base ligand, a yellow needle shaped crystal was chosen using a polarizing microscope and was mounted on a glass fiber which was used for data collection. Cell constants and orientation matrices for data collection were obtained by least-squares refinement of diffraction data from 4458 unique reflections. Data were collected to a maximum 2θ value of 58.36° in a series of ω scans in 1° oscillations and integrated using the Stoe X-AREA [39] software package. The data were corrected for Lorentz and Polarizing effects. The structures were solved by direct methods [40] and subsequent difference Fourier maps and then refined on F^2 by a full-matrix least-squares procedure using anisotropic displacement parameters [41]. The atomic factors were taken from the International Tables for X-ray Crystallography [42]. All refinements were performed using the X-STEP32 crystallographic software package [43]. The ORTEP diagram of the molecular structure of the ligand is shown in Fig. 1. Details of the crystal structure analysis and refinement for the ligand are reported in Table 1. Fig. 2, Table 2 and Table 3 show selected bond length, angles and the summary of hydrogen bond parameter, respectively.

4. DNA Binding Studies

4.1. Electronic Absorption Titration

Measurement of the effects of the free ligand and the Cu (II) complex with CT-DNA was used to study their binding ability by electronic spectroscopy. Compounds binding with DNA usually show hypochromism and bathochromism [44]. The corresponding Tris–HCl buffer solution was the reference solution. Equal amounts of DNA were added to both the compound and reference solutions to eliminate the absorbance of DNA while measuring the absorption spectra. The solution obtained by adding DNA to the compounds in Tris–HCl buffer was allowed to equilibrate at room temperature for 5 min and then scanned in the range of 200–600 nm [45,46].

An effective method for the examination of the binding modes of metal complexes with DNA is electronic absorption spectroscopy. In general, hypochromism and a red shift are associated with the binding of metal complexes to DNA, because of the intercalative mode involving a strong stacking interaction between the aromatic chromophore of the complexes and the base pairs of DNA. UV spectroscopy was used to study the potential CT-DNA binding ability of a complex by following the intensity changes of the intraligand π–π* transition band at 232 and 310 nm [47]. The absorption spectra of the ligand and its Cu (II) complex in the absence and presence of CT-DNA are shown in Fig. 3. As shown in the figure, the binding of the ligand to duplex DNA decreases the absorption intensities with significant hypochromisms of about 28.17, 29.02 and 29.4% at 232, 310 and 394 nm, respectively. Meanwhile, the Cu (II) complex absorption bands exhibited hypochromisms of about 54.12% at 240 nm, 40.67 and 35% with partial red shifts of 2 and 1 nm at 310 and 376 nm, respectively, and only a small shift in the 2 nm wavelength. This observation is attributed to a partial intercalative binding [48]. The binding constants (K_b) of L and the complex to CT DNA were determined by monitoring the absorbance changes at 232 (for L) and 240 nm (for the Cu (II) complex) with

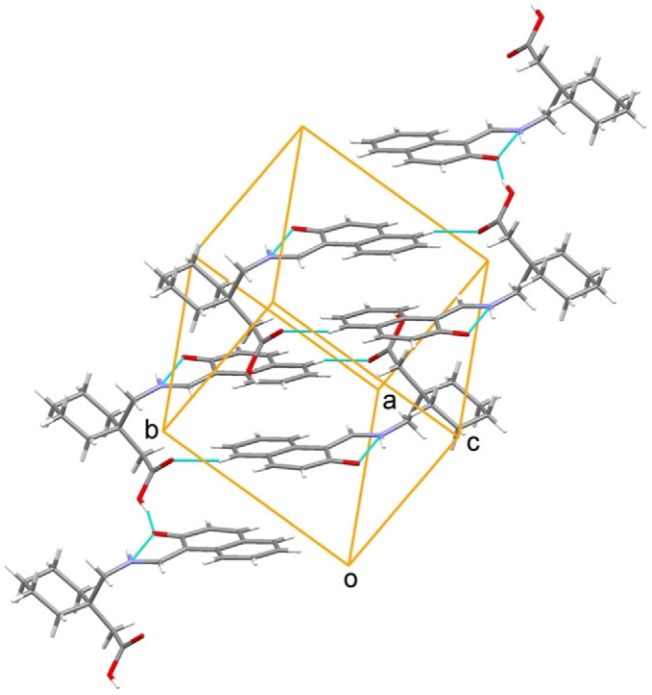

Fig 2. Packing diagram of ligand showing hydrogen bonds.

Table 1
Crystallographic and structure refinement data for ligand.

Empirical formula	$C_{20}H_{23}NO_3$
Formula weight	325.39
Temperature (K)	120 (2)
Wavelength (Å)	0.71073
Crystal system	Triclinic
Space group	$P\bar{1}$
Crystal size (mm^3)	0.35 × 0.15 × 0.05
a (Å)	9.1539 (18)
b (Å)	9.7260 (19)
c (Å)	9.890 (2)
α (°)	89.59 (3)
β (°)	83.21 (3)
γ (°)	71.98 (3)
Volume ($Å^3$)	831.1 (3)
Z	2
Density$_{calc}$ ($g\ cm^{-1}$)	1.300
θ ranges for data collection (°)	2.36–29.18
F (000)	348
Index ranges	$-12 \le h \le 12$ $-13 \le k \le 13$ $-13 \le l \le 13$
Data collected	9195
Unique data, (R_{int})	4458, (0.1207)
Parameters/restrains	225/0
Final R_1/wR_2[a] ($I > 2\sigma(I)$)	0.0871/0.1633
Final R_1/wR_2[a] (all data)	0.1658/0.1958
Goodness-of-fit on F^2 (S)	1.088
Largest diff. peak and hole (e $Å^{-3}$)	0.279, −0.294

[a] $R_1 = \Sigma||F_o| - |F_c||/\Sigma|F_o|$, $wR_2 = [\Sigma(w(F_o^2 - F_c^2)^2) / \Sigma w(F_o^2)^2]^{1/2}$.

Table 2
Selected bond distances (Å) and bond angles (degrees) for ligand.

O(1)—C(9)	1.287 (4)	C(11)—N(1)—C(12)	124.4 (2)
O(2)—C(15)	1.213 (4)	C(15)—C(14)—C(13)	115.4 (2)
O(3)—C(15)	1.312 (4)	O(2)—C(15)—O(3)	123.5 (3)
O(3)—H(3A)	1.00 (4)	O(3)—C(15)—C(14)	113.2 (2)
N(1)—C(11)	1.302 (4)	C(17)—C(16)—C(13)	114.1 (2)
N(1)—C(12)	1.457 (4)	N(1)—C(12)—C(13)	112.8 (2)
C(14)—C(15)	1.508 (4)	O(1)—C(9)—C(10)	121.4 (3)
C(19)—C(20)	1.532 (5)	O(1)—C(9)—C(8)	120.9 (3)

Table 3
Hydrogen bond geometric parameters (Y — A···H — D) for ligand[a].

D—H···A	D—H/Å	A···H/Å	A···D/Å	A···H—D/deg
N(1)—H(1A)···O(1)	0.93 (4)	1.83 (4)	2.579 (3)	135 (3)
O(3)—H(3A)···O(1)$^{\#1}$	1.00 (4)	1.58 (5)	2.563 (3)	168 (4)
C(12)—H(12A)···O(2)	0.9900	2.5600	3.185 (4)	121.00
C(12)—H(12A)···O(2)$^{\#2}$	0.9900	2.5300	3.444 (4)	153.00
C(16)—H(16B)···N(1)	0.9900	2.5600	2.952 (4)	104.00

[a] Symmetry codes: #1: 1 + x,y,z; #2: 2 − x, −y, −z.

increasing DNA concentrations in order to quantitatively compare the affinity of the ligand and complex towards DNA. The data were then fit into the following equation and the intrinsic binding constant, K_b, was calculated according to Eq. (1) [49].

$$\frac{[DNA]}{(\varepsilon_a-\varepsilon_f)}=\frac{[DNA]}{(\varepsilon_b-\varepsilon_f)}+\frac{1}{K_b\,(\varepsilon_b-\varepsilon_f)} \quad (1)$$

where [DNA] is the concentration of DNA in base pairs and the apparent absorption coefficient, ε_a, corresponds to A_{obs}/[compound], ε_f refers to the extinction coefficient of the free compound and ε_b is the extinction coefficient of the compound when fully bound to DNA. The plot of [DNA] / ($\varepsilon_a - \varepsilon_f$) vs. [DNA] (Fig. 3) gave a slope and intercept equal to 1 / ($\varepsilon_b - \varepsilon_f$) and 1 / K_b($\varepsilon_b - \varepsilon_f$), respectively. K_b is the ratio of the slope to the intercept. The observed values of K_b also indicate that the ligand and the Cu (II) complex bind to DNA via a partial intercalative mode [50,51]. The magnitudes of the intrinsic binding constants (K_b) were calculated to be 1.53×10^4 and 3.71×10^5 M^{-1} for the ligand and the Cu complex, respectively. The calculated values of K_b also show that the ligand and the Cu (II) complex bind to DNA via a partial intercalative mode. The complex showed more hypochromicity than the ligand, indicating that the binding strength of the Cu (II) complex is stronger than that of the free ligand. Though it has been found that the compounds can bind to DNA by intercalation from the electronic absorption studies, the binding mode needs to be proved through some more experiments.

From the values of the binding constant (K_b), free energy (ΔG) of the compound–DNA complex was calculated using Eq. (2):

$$\Delta G = -RT\ln K_b \quad (2)$$

Binding constants are a measure of the compound–DNA complex stability while the free energy indicates the spontaneity/non-spontaneity of compound–DNA binding. Free energies of ligand and Cu complex were evaluated as negative values (−5.21 and −6.04 kJ mol^{-1}), showing the spontaneity of compound–DNA interaction. However, these results indicate that the Cu complex binds to DNA more spontaneously compared to the ligand.

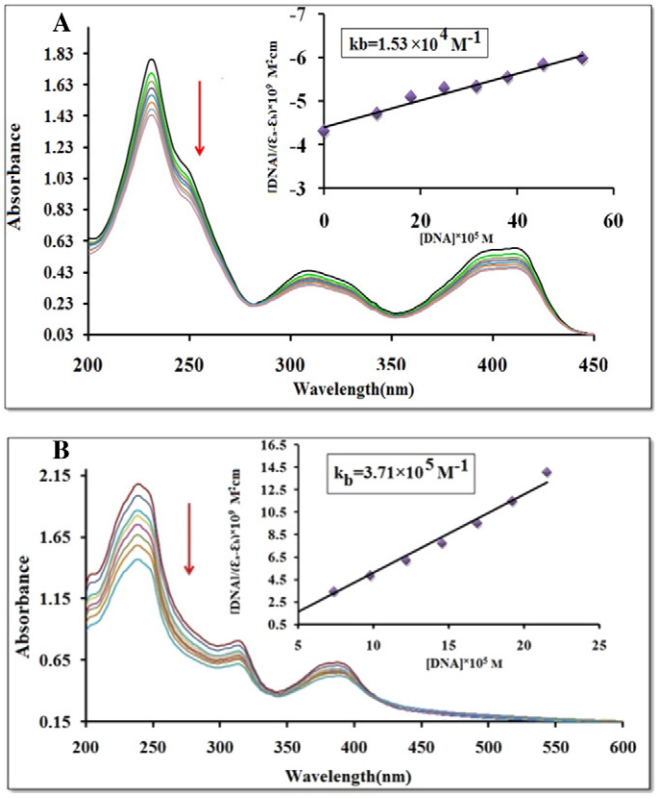

Fig 3. Absorption spectra of ligand (A), and complex (B) in buffer solution (5 mM Tris–HCl/50 m M NaCl at pH 7.4) upon addition of CT DNA. [Ligand] = 4×10^{-5} mol L^{-1}, [DNA] = 0–3.1×10^{-5} mol L^{-1}. [Complex] = 8×10^{-4} mol L^{-1}, [DNA] = 0–2.1×10^{-5} mol L^{-1}. Arrow shows that the absorption intensities decrease upon increasing DNA concentration. Inset: plots of [DNA] / [$e_a - e_f$] vs. [DNA] for the titration of 1a and 1b with CT-DNA.

4.2. Fluorescence Studies of Competitive Interaction of the Compounds with MB-Ds-DNA

No emission band was observed in the fluorescence measurement of the ligand and copper (II) complex with or without CT-DNA at ambient temperature in aqueous solutions. Therefore, the binding of compounds with CT-DNA cannot be directly shown in the emission spectra. To further investigate the interaction mode of the ligand and complex with DNA, the competitive binding experiment was performed using MB as a probe. A competitive study using MB was carried out to support the spectral results. MB is a well-known intercalator, often used as a spectral probe to establish the mode of binding of small molecules to double-helical DNA. A photosensitizer drug, methylene blue (MB), shows promising applications in biological straining and diagnosis of diseases including carcinoma [52–54]. Intense fluorescent light is emitted by MB in the presence of DNA due to the strong intercalation between adjacent DNA base pairs. Reduction of the number of binding sites on the DNA available to MB causes quenching. Following binding with DNA, MB fluorescence decreases because of intercalation [55]. The fluorescence spectra of DNA–MB ligand and DNA–MB complex, the mixture of different concentrations of the compound and DNA–MB were measured using pH 7.4 Tris–HCl buffer. The emission spectra of the MB–DNA solution upon titration with the compounds are shown in two cases, which illustrate that MB–DNA solution emission bands slightly decrease in intensity as the concentration of the compounds increases. The slight decrease of the fluorescence intensity is known to be due to releasing free small MB molecules from the DNA–MB complex, demanding the formation of metal complex–DNA instead of intercalator MB. A complete recovery of MB means the probe fluorescence intensity is sufficiently close to the corresponding pure MB fluorescence intensity [56]. This was not observed in our experiments (Fig. 4). Our studies demand a partial replacing of MB by the two compounds from the MB–DNA system, which is a partial intercalative mode of binding between the title compounds and CT-DNA.

4.3. Melting of DNA Helix in Interaction with the Ligand and Copper Complex

Denaturation of double-stranded DNA (dsDNA) is a very significant phenomenon involving biological, chemical and physical subsequences [57]. The melting temperature (T_m) of DNA is defined as the temperature at which 50% of double strand becomes single stranded. This has been determined as the midpoint of the optically detected transition curves. Moreover, the melting of DNA is an important tool for studying the interaction of transition metal ion with nucleic acid. In addition, the DNA melting experiment is useful in establishing the extent of intercalation. Thus, DNA melting temperature was determined by monitoring

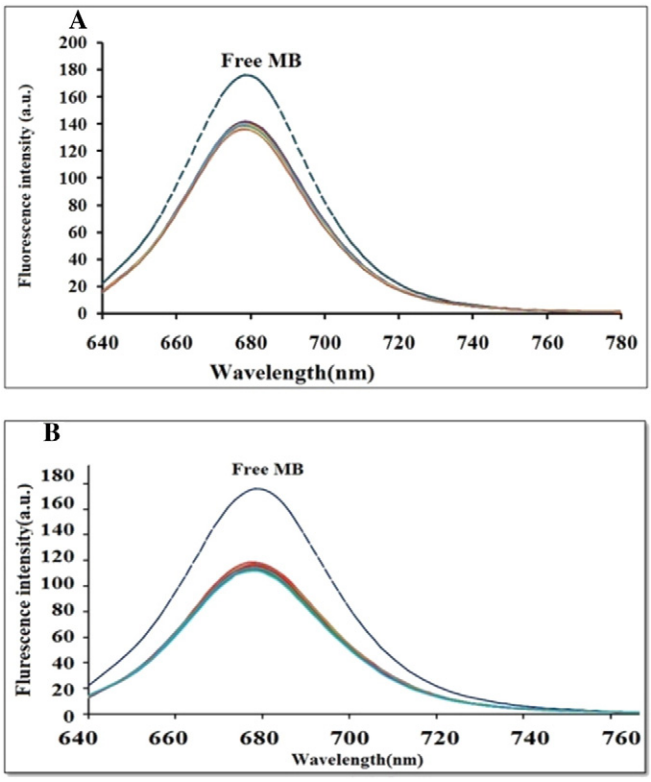

Fig. 4. The emission spectra of the DNA–MB system, in the presence of: ligand (A) and Cu complex (B), [DNA] = 2.5×10^{-5} mol L^{-1}, [ligand] = 0–4.5×10^{-6} mol L^{-1}, [MB] = 5×10^{-6} mol L^{-1}, [DNA] = 2.5×10^{-5} mol L^{-1}, [complex] = 0–5×10^{-6} mol L^{-1}, [MB] = 5×10^{-6} mol L^{-1}. The arrow shows that the emission intensity changes upon increasing complex concentration.

the absorption intensity of CT-DNA at 260 nm in the temperature range from 25 to 100 °C both in the absence and presence of the ligand and copper (II) complex [58]. Commonly, a ΔT_m of a few degrees is considered evidence of an interaction involving groove and /or electrostatic binding to the phosphate groups [59]. According to the literature, the intercalation of natural or synthetic compounds results in the stabilization of the DNA double helix, due to the stabilizing stacking interactions, followed by a considerable increase in the melting temperature of DNA [60,61]. The thermal denaturation profile of CT-DNA in the absence and presence of the ligand and complex are presented in Fig. 5. Here, the T_m of CT-DNA was found to be 81.62 °C in buffer while, the T_m of the DNA increased to 84.23 °C for the ligand and 85.61 °C for the Cu complex following the addition of the ligand and Cu (II) complex. This increase corresponds to that observed for a partial intercalative [62], suggesting partial intercalation of the two compounds and thus supports the results obtained from the absorption and fluorescence studies.

5. Protein Binding Studies

5.1. Electronic Absorption Titration

Many types of medicines and important chemical substances target proteins. As the most abundant protein in the blood circulatory system, serum albumin (SA), plays important parts in the transport of drugs and metal ions throughout the blood stream. Furthermore, proteins function as disposers of a variety of endogenous and exogenous substances including fatty acids and medicinal drugs [63]. Given its low cost, ready availability and structural homology with human serum albumin (HSA), which has a tryptophan at position 214, bovine serum albumin is the most comprehensively studied serum albumin [64]. Thus, the examination of the interaction of potential metallo drugs with BSA is important. Binding to these proteins can provide drug transportation

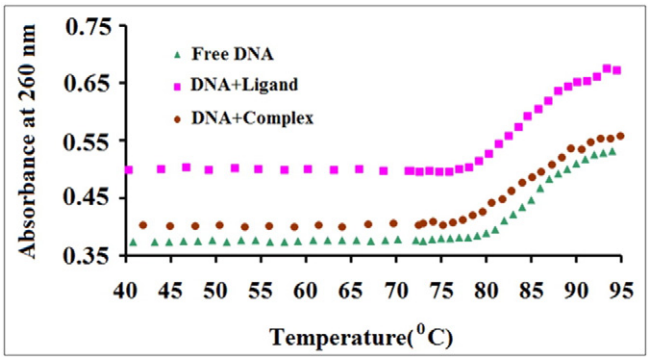

Fig. 5. Plots of the changes of absorbance at 260 nm of CT-DNA (7.5×10^{-6} mol L^{-1}) on heating in the absence and presence of the ligand and complex (3.75×10^{-6} mol L^{-1}) in 5 mM Tris–HCl with 50 Mm NaCl.

paths and suggest new approaches to drug design, making it a significant field of research in life sciences, chemistry, and clinical medicine. A simple and pertinent method used in the investigation of structural changes and exploration of complex formation is UV–vis absorption measurement [65,66]. Two types of quenching mechanism, that is, dynamic and static quenching, can occur. Only the absorption spectra of the excited state fluorescence molecule change in dynamic quenching mechanism. However, the change in absorption spectrum of fluorophore is induced by the formation of non-fluorescence ground state complex [67]. Absorption spectra were used to study the binding of the ligand and Cu (II) complex with bovine serum albumin (BSA). The absorption spectra of BSA occurred at 278 nm during the addition of the ligand and Cu (II) complex, as observed in Fig. 6. The absorption

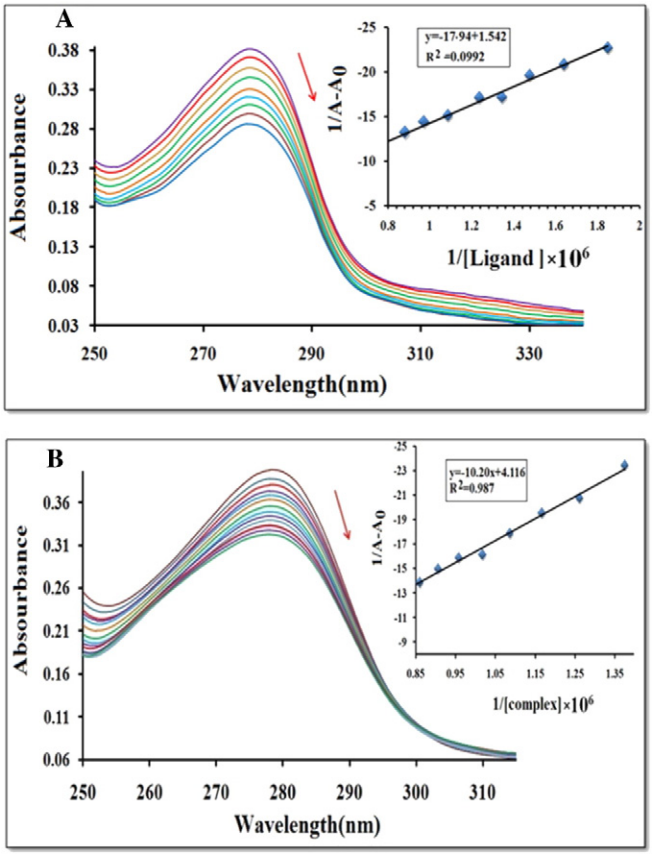

Fig. 6. Electronic absorption spectra of BSA (8×10^{-6} mol L^{-1}) in the absence and presence of different concentrations of the ligand (0–1.8 μM) (A) and complex (0–2.5 μM) (B). The arrow shows the direction of change in absorbance upon increasing the concentrations of the ligand and complex.

spectrum of BSA is strongly red shifted due to the specific binding of two compounds. This red shift and the decrease in absorption intensity indicate the interaction between the ligand and Cu (II) complex with subdomain IIA in a non-planar conformation BSA [68]. UV spectroscopy was used to calculate the overall binding constants, as reported in [69,70]. The ratio of the intercept to slope of the plots of $1 / (A - A_0)$ (where A_0 is the initial absorbance of the free BSA at 278 nm, and A is the absorbance of BSA in the presence of different concentrations of the ligand and/or Cu (II) complex) vs. 1/[ligand] and 1/[Cu (II) complex], which are linear lines, is used to obtain the binding constant (K_b). The values of binding constant (K_b), were 8.6×10^4 for the ligand and 8.5×10^5 for the Cu complex, respectively. However, K_b values show that BSA can be considered a good carrier for the transfer of these compounds in vivo [71]. It is noted that the K_b of 10^4–10^6 M^{-1} is acceptable for drug carriers in blood [72].

5.2. Fluorescence Quenching Studies of BSA

Fluorescence spectroscopy was used to investigate the quenching mechanism, mode and strength of the interaction of BSA with the ligand and the Cu (II) complex. The strong fluorescence properties of BSA are due to the aromatic amino acids (Trp, Tyr, and Phe). The intrinsic fluorescence intensity of BSA, when excited at 280 nm, is mainly due to the tryptophan residues, Trp-134 and Trp-212. On more exposure to the environment, fluorescence quenching may result from ground state complex formation, energy transfer and dynamic quenching processes [73]. Dynamic quenching refers to a process in which the fluorophore and the quencher come into contact during the lifetime of the excited state, whereas static quenching refers to fluorophore–quencher complex formation when different amounts of the ligand and the Cu (II) complex are added to a fixed concentration of BSA. Under the conditions of fixed pH, temperature and ionic strength, a remarkable decrease in the fluorescence intensities of BSA was observed, without any significant shift in the position of the maximum emission wavelength (Fig. 7), indicating that the interaction of the two compounds with BSA could cause changes in protein secondary structure leading to changes in trp environment of BSA [74,75]. In order to understand quantitatively the quenching mechanism, the fluorescence quenching data were analyzed by the linear Stern–Volmer Eq. (3):

$$F_0/F = 1 + K_{sv}[Q] = 1 + K_q\tau_0[Q] \quad (3)$$

where F_0 and F are the fluorescence intensities of the fluorophore in the absence and presence of a quencher, respectively, K_{sv} is a linear Stern–Volmer quenching constant, [Q] is the quencher concentration, k_q is the bimolecular quenching rate constant and equal to $k_q = K_{sv} / \tau_0$ and τ_0 is the average lifetime of the fluorophore in the absence of the quencher. τ_0 is equal to 10–8 s for tryptophan fluorescence in proteins [76]. The plots of F_0/F_{sv} [Q] represent a good linear relationship (Fig. 7). The K_{SV} values, 5.6×10^4 M^{-1} for the ligand and 7.9×10^4 M^{-1} for the Cu complex are almost coincident. It is known that a linear Stern–Volmer plot represents a single quenching mechanism, either static or dynamic. The obtained values of quenching constants (k_q), were 2.8×10^{12} for the ligand and 3.9×10^{12} for the Cu complex, respectively. However, the maximum scatter collision quenching constant, K_q, for various quenchers with the biopolymer is 2×10^{10} M^{-1} s^{-1} [77]. Thus, the rate constant calculated by the protein quenching procedure is 100-fold higher than K_q of the scatter procedure. This finding indicates that a static quenching mechanism is operative [78,79].

5.3. Binding Constant and Number of Binding Sites and Gibbs Free Energy Values

Small molecules bind independently to a set of equivalent sites on a macromolecule. The binding constant K_b and the number of binding sites per albumin molecule can be determined according to the

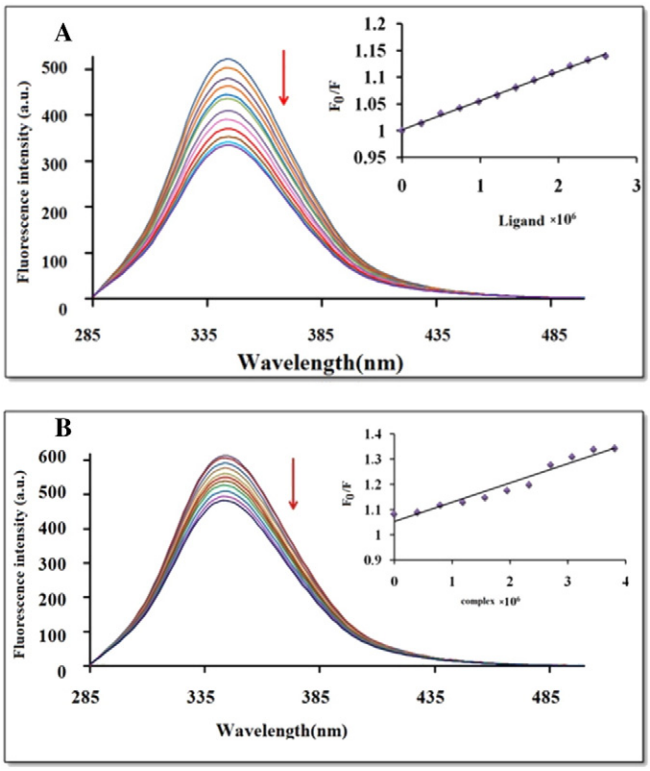

Fig 7. Emission spectra of BSA upon the titration of: ligand (A) and complex (B). [BSA] = 5×10^{-6} mol L^{-1}, [ligand] = 0–4.55×10^{-6} mol L^{-1}, [complex] = 0–5.58×10^{-6} mol L^{-1}. Arrow shows the change upon the increasing complex concentration. Inset: plots of F_0/F_{SV} [ligand] and [complex] for the titration of the complex to BSA.

Scatchard Eq. (4): [80].

$$\mathrm{Log}[(F_0 - F)/F] = \log K + n \log[Q] \quad (4)$$

K_b and n values were obtained from the intercept and slope through the double logarithm regression curve of $\log[(F_0 - F) / F]$ vs. log[Q]. As shown in Fig. 8, the binding constants K and Gibbs free energy values were (6.3×10^4 M^{-1}, −65.4 kJ mol^{-1}) for the ligand, and (1.02×10^5 M^{-1}, −68.3 kJ mol^{-1}) for the Cu complex. In addition, the Gibbs free energy values were obtained from Eq. (2). The negative values of ΔG through fluorescence results also supported the UV-results of free energy changes and indicated the spontaneity of the compounds–BSA binding. The plot exhibited a good linear relationship with the linear correlation coefficient of 0.994 and 0.981. The values of K_q and K_{bin} for the ligand and complex suggested that the Cu complex interacts with BSA more strongly than the ligand. The numbers of binding stoichiometry/site (n) were approximately 0.983 for the ligand and 0.894 for the complex, which indicated that there was one binding site for two compounds on the BSA molecular. In general, three intrinsic proteins with intrinsic characteristics, including tryptophan, tyrosine, and phenyl alanine residues cause the fluorescence of proteins. In fact, the intrinsic fluorescence of many proteins is mostly contributed by tryptophan alone. The emission intensity depends on the extent of exposure of the two tryptophan side chains [81]. There are two tryptophan residue intrinsic fluorescence in the BSA molecule, as reported in the literature. One of these is Trp-213 in a hydrophobic binding pocket of the protein and the other is located on the surface of the hydrophilic region, namely Trp134. The intrinsic fluorescence of BSA is mainly due to Trp213, because Trp134 is more exposed to a hydrophilic environment [82]. These two compounds may not rapidly penetrate the hydrophobic interior of a protein and only those tryptophan residues on the surface of protein BSA are quenched. Therefore, it is reasonable to suspect that

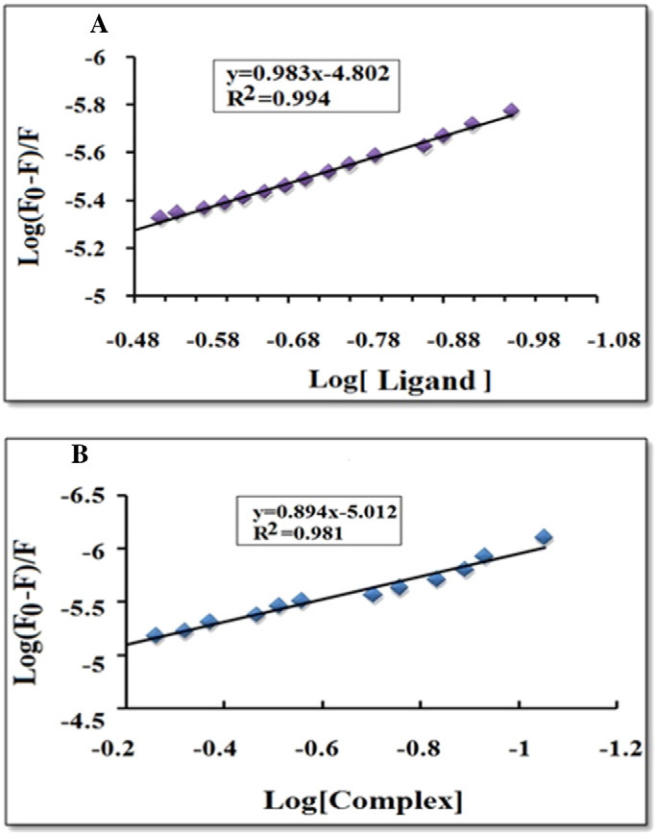

Fig 8. Scatchard plots of log[($F_0 - F$) / F] vs. log[Q] for determination of the complex–BSA binding constant and the number of binding sites on BSA for ligand (A) and complex (B).

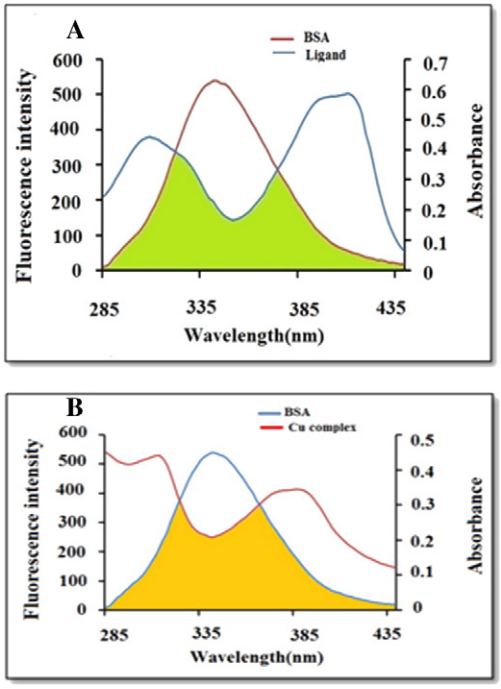

Fig 9. Spectral overlaps of the absorption spectra of the ligand (A) and Cu complex (B) with the fluorescence spectra of BSA. [BSA] = [ligand] = 3.0 × 10–7 mol L^{-1} and [BSA] = [Cu complex] = 2.8 × 10–7 mol L^{-1}, T = 298 K, and pH 7.4; λ_{ex} = 280 nm, λ_{em} = 285–435 nm.

the two compounds most likely bind to BSA through the surface site Trp213 [83].

5.4. Energy Transfer from BSA to the Ligand and Cu Complex

The overlap of the UV–vis absorption spectrum of the ligand and complex with the fluorescence emission spectrum of BSA in the wavelength range of 285 to 440 nm [84] is shown in Fig. 9. The importance of the energy transfer in biochemistry is that the efficiency of transfer can be used to evaluate the distance between the ligand and the tryptophan residues in the protein. This considerable overlap forms the basis of fluorescence resonance energy transfer (FRET) [85]. The effective energy transfer from a donor to an acceptor will occur under the following conditions: (1) production of fluorescent light with a sufficiently long lifetime by the donor species; (2) a significant overlap between the fluorescence spectrum of the donor and the absorption spectrum of the acceptor; and (3) the closeness of the donor species to the acceptor (the distance of <8 nm) [86]. The energy transfer between the donor and the acceptor is calculated using Eq. (5).

$$E = 1 - F/F_0 = {R_0}^6/({R_0}^6 + r^6) \quad (5)$$

where r is the donor–acceptor distance, F and F_0 are the fluorescence intensities of BSA in the presence and absence of a quencher and R_0 is the critical distance when the transfer efficiency is 50%, which can be calculated based on Eq. (6) [87].

$${R_0}^6 = 8.8 \times 10^{-25} K^2 N^{-4} \Phi J \quad (6)$$

In the above equation, K^2 is the spatial orientation factor of the dipole, N is the refractive index of the medium, Φ is the fluorescence quantum yield of the donor, and J is the overlap integral of the fluorescence spectrum of the donor with the absorption spectrum of the acceptor (Fig. 9). The value of J is calculated using Eq. (7): [88].

$$J = \left[\Sigma F_{(\lambda)} \varepsilon_{(\lambda)} \lambda^4 \Delta\lambda\right] / \left[\Sigma F_{(\lambda)} \Delta\lambda\right] \quad (7)$$

where $F(\lambda)$ is the fluorescence intensity of BSA in the absence of a quencher at wavelength λ and $\varepsilon_{(\lambda)}$ is the molar extinction coefficient of the acceptor at λ. In the present case, K^2 = 2/3, N = 1.336 and Φ = 0.15. Hence, using Eqs. (5)–(7) above, the following parameter can be calculated: $J = 1.24 \times 10^{-14}$ cm^3 L mol^{-1}, R_0 = 2.64 nm, E = 0.361 and r = 2.45 nm for the ligand and $J = 1.08 \times 10^{-14}$ cm^3 L mol^{-1}, R_0 = 2.58 nm, E = 0.148 and r = 3.46 nm for the Cu complex. Obviously, the distance between two compounds and BSA is <8 nm, and $0.5R_0 < r < 1.5R_0$, implying that the energy transfer from BSA to two compounds occurred with high probability. The bigger r value compared with R_0 again indicates the presence of a static quenching mechanism in the binding of the two complexes to BSA [89].

6. Cytotoxicity Assay

In vitro cytotoxicity of compounds was evaluated by means of the standard MTT-dye reduction assay, which is a broadly used method in biological evaluation. Recently, new metal complexes were assessed using this method [90,91]. MTT [3-(4,5-dimethylthiazol-2-yl)-2,5-diphenyl-tetrazolium bromide] colorimetric assay was used to evaluate the cytotoxic activity of the ligand and Cu complex. This test is based on the metabolic reduction of soluble MTT by mitochondrial enzyme activity of viable tumor cells. The product is an insoluble colored formazan, which can be quantified spectrophotometrically after dissolution in dimethylsulfoxide (DMSO). In order to perform the cytotoxicity assay, 200 μl of cells (5×10^4 cells ml^{-1}) was seeded in 96 well micro plates and incubated for 24 h (37 °C, 5% CO_2 air humidified). Subsequently, 20 μl of prepared concentrations of each compound was added to the wells. The compounds were dissolved in DMSO before being added to the culture media. Control groups contained DMSO at the same

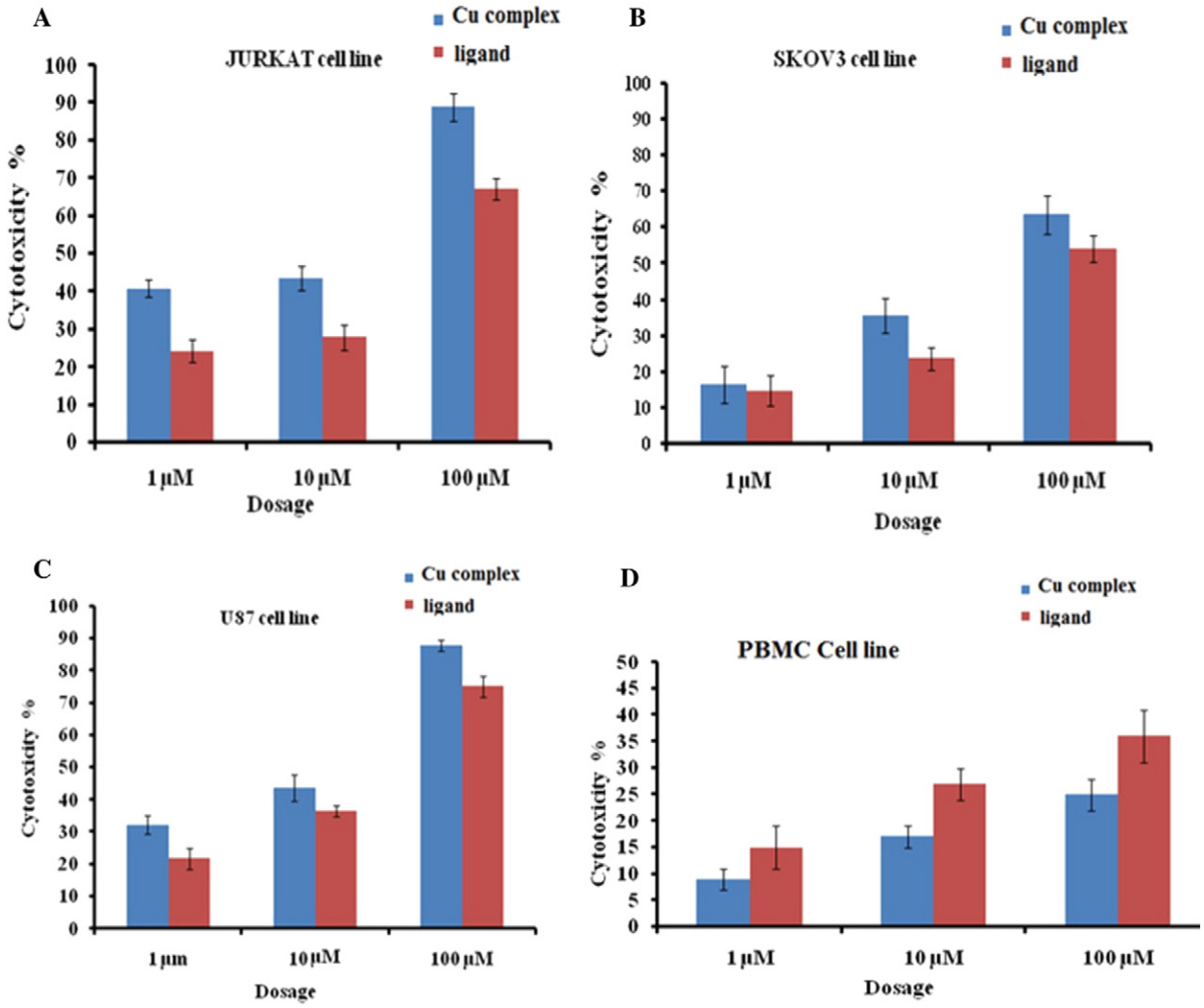

Fig 10. Dose-dependent cytotoxic activity of the ligand and Cu complex against JURKAT (A), SKOV3 (B), and U87 (C) cancer cell lines and the normal PBMC cell line (D) at concentrations of 10 and 100 µM. Results are the mean ± SD of three independent experiments. All data are significant differences from untreated control by $p < 0.05$.

concentration [0.5% (v/v)] of treated groups. After 48 h of incubation, 20 µl of MTT solution (5 mg ml^{-1} in phosphate buffer solution) was added and the plates were incubated for another 3 h. 150 µl of the medium containing MTT were then gently replaced by DMSO and pipetted to dissolve any formazan crystal formed. Absorbance was then determined at 560 nm using an ELISA plate reader (Awareness Technology Inc., stat fax 2100). Results were generated from three independent experiments and each experiment was performed in triplicate. IC_{50} (concentration which inhibits cell growth by 50%) values of ligand and Cu complex against each tested cell line was calculated using non-linear regression of concentration-response curves. The selectivity index (SI) was also calculated based on the IC_{50} ratio of normal human peripheral blood mononuclear cells (PBMCs) and cancer (JURKAT, SKOV3 and U87) cells. SI value indicates selectivity of the sample to the cell lines tested. Samples with SI values >2 were considered to have a high selectivity [92].

6.1. Selective Cancer-cell Cytotoxic Activity

The ligand and Cu complex were tested for cytotoxicity against 3 human cancer cell lines. Both compounds showed low toxicity (IC_{50} > 300 µM) against normal peripheral blood mononuclear cells (PBMCs), but demonstrated a high selective cytotoxicity against 3 human cancer cell lines. The ligand showed cytotoxicity against JURKAT, SKOV3, and U87 cancer cell lines with IC_{50} values of 60.82, 87.9 and 48.35 µM, respectively. Notably, the Cu complex exerted higher cytotoxicity against JURKAT, SKOV3, and U87 cancer cell lines with IC_{50} values of 21.27, 64.98 and 28.4 µM, respectively (Fig. 10 and Table 4).

As depicted in Fig. 10, both compounds exhibited significant dose-dependent inhibition on proliferation and viability of different cancer cells. Selectivity of the cytotoxic activity was determined by comparing the cytotoxic activity (IC_{50}) of the compound against each cancer cell with that of the normal cell line PBMC (Table 4).

7. Conclusions

We have synthesized a novel Schiff base derived from the gabapentin drug and copper (II) complex containing ligand. The structure of the ligand was characterized by X-ray crystallography and the copper (II) complex was characterized by FT-IR, ESI-MASS and other methods. The binding interaction of two biologically relevant

Table 4
Selective cytotoxicity of ligand and Cu complex against 3 different cancer cell lines.

Cell line	Compound	IC_{50}	SI
JURKAT	Cu complex	21.27	14
	Ligand	60.82	5
SKOV3	Cu complex	64.98	4.6
	Ligand	87.9	3.5
U87	Cu complex	28.4	10.5
	Ligand	48.35	6.2

compounds with calf thymus DNA, bioactivity investigation by UV–vis and fluorescence spectroscopy, and other spectroscopic measurements unambiguously suggested the binding of a partial intercalative by the probe with the DNA. The reactivity towards BSA revealed that the quenching of BSA fluorescence by two compounds was of the static type. The cytotoxic studies show that the two compounds exhibit high selective and dose-dependent cytotoxic activity against three different cancer cell lines. In addition, the results of cytotoxicity revealed that the Cu complex is more effective than its free ligand under identical experimental conditions. It is interesting that the DNA and protein binding abilities of the two compounds are consistent with in vitro cytotoxic activity and follow the order of Cu complex > ligand.

Acknowledgements

We greatly appreciate the financial support of Isfahan University of Technology (IUT) and Medical Biotechnology, and the School of Medicine, Mashhad University of Medical Sciences. Crystallography was supported by the Department of Chemistry, Shahid Beheshti University.

Appendix A. Supplementary material

CCDC 1422955 contains the supplementary crystallographic data for the ligand. This data can be obtained free of charge from the Cambridge Crystallographic Data Center via www.ccdc.cam.ac.uk/data_request/cif. Supplementary data associated with this article can be found in the online version, at doi: http://dx.doi.org/10.1016/j.jphotobiol.2016.06.022.

References

[1] W.C. Loscher, Current status and future in the pharmacology of epilepsy, Trends Pharmacol Sci. 23 (2002) 113–118.
[2] K. Ananda, S. Aravinda, P.G. Vasudev, K.M.P. Raja, H. Sivaramakrishnan, K. Nagarajan, N. Shamala, P. Balaram, Curr. Sci. 85 (7) (2003) 1002–1011.
[3] P.H. McCabe, Role of levetiracetam in the treatment of epilepsy, Expert Opinion Pharmacother. 1 (2000) 633–674.
[4] M. Elmastas, I. Gulcin, S. Beydemir, H.Y. Kufreviogluo Aboul-Enein, A study on the in vitro antioxidant activity of juniper seeds extracts, Anal Lett. 39 (2006) 47–65.
[5] G. Regesta, P. Tanganelli, Clinical aspects and biological bases of drug-resistant epilepsies, Epilepsy Res. 34 (1999) 109–122.
[6] Gabapentin as a possible treatment, J Headache Pain. 1 (2000) 155–161.
[7] A. Bilici, İ. Kaya, F. Doğan, Monomer/polymer Schiff base copper (II) complexes for catalytic oxidative polymerization of 2,2′-dihydroxybiphenyl, J. Polym. Sci. A Polym. Chem. 47 (2009) 2977–2984.
[8] U. El-Ayaan, A.A.M. Abdel-Aziz, Eur. J. Med. Chem. 40 (2005) 1214.
[9] M. Sonmez, I. Berber, E. Akbas, Eur. J. Med. Chem. 41 (2006) 101.
[10] E. Canpolat, M. Kaya, J. Coord. Chem. 57 (2004) 1217.
[11] R.L. Lucas, M.K. Zart, J. Murkherjee, T.N. Sorrell, D.R. Powell, A.S. Borovik, J. Am. Chem. Soc. 128 (2006) 15476.
[12] P.E. Aranha, M.P. Do Santo, S. Romera, E.R. Dockal, Polyhedron 26 (2007) 1373.
[13] A.A. Soliman1, W. Linert, Monatsh. Chem. 138 (2007) 175.
[14] M. Xie, G. Xu, L. Li, W. Liu, Y. Niu, S. Yan, Eur. J. Med. Chem. 42 (2007) 817.
[15] P. Piotr, B. Bogumil, Spectroscopic studies and PM3 semi empirical calculations of Schiff bases of gossypol with L-amino acid methyl esters, Biopolymers 67 (2002) 61–67.
[16] C. Santini, M. Pellei, V. Gandin, M. Porchia, F. Tisato, C. Marzano, Advances in copper complexes as anticancer agents, Chem. Rev. 114 (2014) 815–862.
[17] R.K. Koiri, S.K. Trigun, S.K. Dubey, S. Singh, L. Mishra, Metal Cu(II) and Zn(II) bipyridyls as inhibitors of lactate dehydrogenase, Biometals 21 (2008) 117–126.
[18] F. Arjmand, M. Muddassir, A mechanistic approach for the DNA binding of chiral enantiomeric L- and D-tryptophan-derived metal complexes of 1,2-DACH: cleavage and antitumor activity, Chirality 23 (2011) 250–259.
[19] A.M. Pyle, T. Morri, J.K. Barton, J. Am. Chem. Soc. 112 (1990) 9432–9434.
[20] J.K. Barton, J.M. Goldberg, C.V. Kumar, N.J. Turro, J. Am. Chem. Soc. 108 (1986) 2081–2088.
[21] F. Arjmand, M. Muddassir, R.H. Khan, Chiral preference of L-tryptophan derived metal-based antitumor agent of late 3d-metal ions (Co (II), Cu(II) and Zn(II)) in comparison to D- and DL-tryptophan analogues: their in vitro reactivity towards CT DNA, 50-GMP and 50-TMP, Eur. J. Med. Chem. 45 (2010) 3549–3557.
[22] D. Jayaraju, A.K. Kondapi, Anti-cancer copper salicylaldoxime complex inhibits topoisomerase II catalytic activity, Curr. Sci. 81 (2001) 787–792.
[23] C. Marzano, M. Pellei, F. Tisato, C. Santini, Copper complexes as anticancer agents, Anticancer Agents Med. Chem. 9 (2009) 185–211.
[24] Z.C. Liu, B.D. Wang, B. Li, Q. Wang, Z.Y. Yang, T.R. Li, Y. Li, Crystal structures, DNA-binding and cytotoxic activities studies of Cu(II) complexes with 2-oxoquinoline-3-carbaldehyde Schiff-bases, Eur. J. Med. Chem. 45 (2010) 5353–5361.
[25] S. Ramakrishnan, D. Shakthipriya, E. Suresh, V.S. Periasamy, M.A. Akbarsha, M. Palaniandavar, Ternary dinuclear copper(II) complexes of a hydroxybenzamide ligand with diimine coligands: the 5,6-dmp ligand enhances DNA binding and cleavage and induces apoptosis, Inorg. Chem. 50 (2011) 6458–6471.
[26] a) E. Chalkidou, F. Perdih, I. Turel, D.P. Kessissoglou, G. Psomas, J. Inorg. Biochem. 113 (2012) 55–65 (and references cited therein);
b) M.S. Mohamed, A.A. Shoukry, A.G. Ali, Spectrochim. Acta A 86 (2012) 562–570;
c) S. Ramakrishnan, D. Shakthipriya, E. Suresh, V.S. Periasamy, M.A. Akbarsha, M. Palaniandavar, Inorg. Chem. 50 (2011) 6458–6471.
[27] D.K. Chand, H.J. Schneider, A. Bencini, A. Bianchi, C. Giorgi, S. Ciattini, B. Valtancoli, Chem. Eur. J. 6 (2000) 4001–4008.
[28] a) Z.C. Liu, B.D. Wang, B. Li, Q. Wang, Z.Y. Yang, T.R. Li, Y. Li, Eur. J. Med. Chem. 45 (2010) 5353–5361;
b) A.A.A. Abou-Hussein, W. Linert, Spectrochim. Acta. A 95 (2012) 596–609;
c) B.S. Creaven, M. Devereux, A. Foltyn, S. McClean, G. Rosair, V.R. Thangella, M. Walsh, Polyhedron, 29 (2010) 813–822;
d) F. Arjmand, F. Sayeed, M. Muddassir, J. Photochem, Photobiol. B 103 (2011) 166–179.
[29] X.L. Wei, J.B. Xiao, Y.F. Wang, Y.L. Bai, Spectrochim, Spectrochim. Acta A Mol. Biomol. Spectrosc. 75 (2010) 299–304.
[30] F. Arjmand, P. Tewatia, M. Aziz, R.H. Khan, Med. Chem. Res. 19 (2010) 794–807.
[31] S.L. Zhang, G.L.V. Damu, L. Zhang, R.X. Geng, C.H. Zhou, Eur. J. Med. Chem. 55674 (2012) 164–175.
[32] S. Satyanarayana, J.C. Dabroniak, J.B. Chaires, Biochemistry 31 (1992) 9319–9324.
[33] A. Kakanejadifard, F. Esna-ashari, P. Hashemi, A. Zabardasti, Spectrochim. Acta A 106 (2013) 80–85.
[34] K. Nakamoto, Infrared Spectra of Inorganic and Coordination Compounds, 3rd ed. New York, Wiley, 978, pp. 232.
[35] H.E. Smith, J.R. Neergaard, E.P. Burrows, F.M. Chen, J. Am. Chem. Soc. 96 (9) (1974) 2908–2916.
[36] Z.H. Abd El-Wahab, M.M. Mashaly, A.A. Salman, B.A. El-Shetary, A.A. Faheim, J. Spectrochim. Acta A 60 (2004) 2861–2873.
[37] A.B.P. Lever, Inorganic Electronic Spectroscopy, second ed. Elsevier, Amsterdam, 1984.
[38] A.B.P. Lever, Inorganic Electronic Spectroscopy, Elsevier Science Publishers BV, Amsterdam, Oxford, New York, Tokyo, 1984.
[39] Stoe & Cie, X–AREA: Program for the Acquisition and Analysis of Data, Version 1.30, Stoe & Cie GmbH, Darmatadt, Germany, 2005.
[40] G.M. Sheldrick, SHELX97. Program for Crystal Structure Solution, University of Göttingen, Germany, 1997.
[41] G.M. Sheldrick, SHELX97. Program for Crystal Structure Refinement, University of Göttingen, Germany, 1997.
[42] International Tables for X-ray Crystallography, CKluwer Academic Publisher, Doordrecht, The Netherlands, 1995.
[43] Stoe & Cie, X-STEP32: Crystallographic Package, Version 1.07b, Stoe & Cie GmbH, Darmstadt, Germany, 2000.
[44] B. Peng, H. Chao, B. Sun, H. Li, F. Gao, L.-N. Ji, J. Inorg. Biochem. 100 (2006) 1487.
[45] M.E. Reichmann, S.A. Rice, C.A. Thomas, P. Doty, J. Am. Chem. Soc. 76 (1954) 3047.
[46] Y. Ni, S. Du, S. Kokot, Interaction between quercetin–copper(II) complex and DNA with the use of the neutral red dye fluorophor probe, Anal. Chim. Acta 584 (2007) 19–27.
[47] T.M. Kelly, A.B. Tossi, D.J. McConnell, T.C. Strekas, Nucleic Acids Res. 13 (1985) 6017-6.
[48] D.S. Raja, N.S.P. Bhuvanesh, K. Natarajan, Eur. J. Med. Chem. 47 (2012) 73–85.
[49] A. Wolfe, G.H. Shimer, T. Meehan, Biochemistry 26 (1987) 6392–6396.
[50] P.R. Reddy, A. Shilpa, N. Raju, P. Raghavaiah, J. Inorg. Biochem. 105 (2011) 1603–1612.
[51] D.S. Raja, N.S.P. Bhuvanesh, K. Natarajan, Inorg. Chem. 50 (24) (2011) 12852–12866.
[52] E. Tuite, B. Norden, J. Am. Chem. Soc. 116 (1994) 7548.
[53] B. Meric, K. Kerman, D. Ozkan, P. Kara, S. Erensoy, U.S. Akarca, M. Mascini, M. Ozsoz, Talanta 56 (2002) 837.
[54] M. Wainwright, R.M. Giddens, Dyes Pigments 57 (2003) 245.
[55] S. Nafisi, A.A. Saboury, N. Keramat, J.F. Neault, H.A. Tajmir-Riahi, J. Mol. Struct. 35 (2007) 827.
[56] L.Z. Zhang, P. Cheng, Inorg. Chem. Commun. 7 (2004) 392.
[57] A.L. Lehninger, D.L. Nelson, M.M. Cox, Principles of Biochemistry, New York, 1993.
[58] C.V. Kumar, E.H. Asuncion, J. Am. Chem. Soc. 115 (1993) 8547.
[59] G.A. Neyhart, N. Grover, S.R. Smith, W. Kalsbeck, T.A. Fairley, M. Cory, H.H. Thorp, J. Am. Chem. Soc. 115 (1993) 4423.
[60] S.-Y. Deng, L.-N. Ji, Z.-W. Mao, J. Inorg. Biochem. 100 (2006) 1586.
[61] G.A. Neyhart, N. Grover, S.R. Smith, W.A. Kalsbeck, T.A. Fairly, M. Cory, H.H. Thorp, J. Am. Chem. Soc. 115 (1993) 4423–4428.
[62] G. Cohen, H. Eisenberg, Biopolymers 8 (1969) 45.
[63] N. Zhou, Y.Z. Liang, P. Wang, J. Mol. Struct. 872 (2008) 190–196.
[64] K.S. Ghosh, S. Sen, B.K. Sahoo, S. Dasgupta, Biopolymers 91 (2009) 737–744.
[65] T.T. Chen, S.J. Zhu, H. Cao, Y.F. Shang, M. Wang, G.Q. Jiang, Y.J. Shia, T.H. Lu, Studies on the interaction of salvianolic acid B with human hemoglobin by multi-pectroscopic techniques, Spectrochim. Acta A 78 (2011) 1295–1301.
[66] B. Valeur, J.C. Brochon, New Trends in Fluorescence Spectroscopy, sixth ed. Springer Press, Berlin, Germany, 1999 25–28.
[67] H.Y. Liu, Z.H. Xu, X.H. Liu, P.X. XI, Z.Z. Zeng, Chem. Pharm. Bull. 57 (2009) 1237.
[68] Y. Hu, Y. Yang, C. Dai, Y. Liu, X. Xiao, Biomacromolecules 11 (2010) 106–112.
[69] S. Nafisi, G.B. Sadeghi, A. PanahYab, J. Photochem. Photobiol. B 105 (2011) 198–202.
[70] M. Anjomshoa, S.J. Fatemi, M. Torkzadeh-Mahani, H. Hadadzadeh, Spectrochim. Acta A Mol. Biomol. Spectrosc. 127 (2014) 511–520.
[71] D.M. Byler, H. Susi, Examination of the secondary structure of proteins by deconvolved FT-IR spectra, Biopolymers 25 (1986) 469–487.

[72] C.N.N. soukpoe-Kossi, R. Sedaghat-Herati, C. Ragi, S. Hotchandani, H.A. Tajmir-Riahi, Int. J. Biol. Macromol. 40 (2007) 484–490.
[73] N.S. Quiming, R.B. Vergel, M.G. Nicolas, J.A. Villanueva, J. Health Sci. 51 (2005) 8–15.
[74] S.S. Bhat, A.A. Kumbhar, H. Heptullah, A.A. Khan, V.V. Gobre, S.P. Gejji, V.G. Puranik, Inorg. Chem. 50 (2011) 545–558.
[75] Y. Shi, H. Liu, M. Xu, Z. Li, G. Xie, L. Huang, Z. Zeng, Spectrochim. Acta A 87 (2012) 251–257.
[76] Y.J. Hu, Y. Liu, J.B. Wang, X.H. Xiao, S.S. Qu, J. Pharm. Biomed. Anal. 36 (2004) 915–919.
[77] C.Y. Gao, X. Qiao, Z.Y. Ma, Z.G. Wang, J. Lu, J.L. Tian, J.Y. Xu, S.P. Yan, Dalton Trans. 41 (2012) 12220.
[78] H.Y. Liu, Z.H. Xu, Chem. Pharm. Bull. 57 (2009) 1237–1242.
[79] P. Kalaivani, R. Prabhakaran, M.V. Kaveri, R. Huang, R.J. Staples, K. Natarajan, Inorg. Chim. Acta 405 (2013) 415–426.
[80] P. Banerjee, S. Ghosh, A. Sarkar, S.C. Bhattacharya, J. Lumin. 131 (2011) 316–321.
[81] T. Peters, Serum albumin, Adv. Protein Chem. 37 (1985) 161–245.
[82] A. Sulkowska, Interaction of drugs with bovine and human serum albumin, J. Mol. Struct. 614 (2002) 227–232.
[83] N. Tayeh, T. Rungassamy, J.R. Albani, Fluorescence spectral resolution of tryptophan residues in bovine and human serum albumins, J. Pharm. Biomed. Anal. 50 (2009) 107–116.
[84] B. Chakraborty, S. Basu, J. Lumin. 129 (2009) 34–39.
[85] L.A. Sklar, B.S. Hudson, R.D. Simoni, Biochemistry 16 (1977) 5100–5108.
[86] Y. Zhang, S. Shi, M. Peng, J. Lumin. 132 (2012) 1921–1928.
[87] F. Deng, Y. Liu, J. Lumin. 132 (2012) 443–448.
[88] (a) F. Samari, M. Shamsipur, B. Hemmateenejad, T. Khayamian, S. Gharaghani, Eur. J. Med. Chem. 54 (2012) 255–263;
(c) N. Shahabadi, M. Maghsudi, S. Rouhani, Food Chem. 135 (2012) 1836–1841.
[89] F.L. Cui, J. Fan, D.L. Ma, M.C. Liu, X.G. Chen, Z. Hu, Anal. Lett. 36 (2003) 2151–2166.
[90] J. Zhang, L. Ma, H. Lu, Y. Wang, S. Li, S. Wang, G. Zhou, Eur. J. Med. Chem. 58 (2012) 281–286.
[91] N. Miklásová, E. Fischer-Fodor, P. Lönnecke, C.I. Tomuleasa, P. Virag, M.P. Schrepler, R. Miklás, L.S. Dumitrescu, E. Hey-Hawkins, Eur. J. Med. Chem. 49 (2012) 41–47.
[92] A. Koch, P. Tamez, J. Pezzuto, D. Soejarto, Evaluation of plants used for antimalarial treatment by the Maasai of Kenya, J. Ethnopharmacol. 101 (2005) 95–99.